Complementary Co-assembling Peptides: From In Silico Studies to In Vivo Application

*Andrea Raspa, Gloria A. A. Saracino, Raffaele Pugliese, Diego Silva, Daniela Cigognini, Angelo Vescovi, and Fabrizio Gelain**

Self-assembling biomaterials offer an unprecedented chance of successfully facing most of the challenges of various biomedical fields, and, in particular, of tissue engineering. Nonetheless co-assembling peptides (CAPs), taking advantage of the theory and empirical findings developed for self-assembling peptides, could provide an even better control over cell cultures, drug delivery, and transplantation therapies. This study follows a "full" bottom-up approach to develop new CAPs for neural tissue engineering applications. After molecular aggregation analysis via coarse-grained simulations, LKLK12, LDLD12, and the functionalized KLPGWSG-LDLD12 CAPs are synthesized and characterized assessing their co-assembled secondary structures, the biomechanical properties of the obtained hydrogels, and the morphological features of the assembled nanofibers. The biological influence on viability and differentiation of human and murine neural stem cells are tested in vitro and neuroregenerative potentials in complete spinal cord transections are verified in vivo. Upon mixing of CAPs, the spontaneous formation of double layers of β-sheets with a high degree of integration of the two CAP species is demonstrated. The formation of entangled nanofibrous structures give rise to shear-thinning hydrogels. The in vitro results are comparable to a standard state-of-the-art cell culture substrate and nervous regeneration in vivo is enhanced.

1. Introduction

Spinal cord injury (SCI) is one of the main causes of invalidity in young adults. For many years, the loss of sensory and voluntary motor functions after SCI has been thought to be incurable because of the limited regenerative ability of central nervous system (CNS). SCI pathology is determined by the initial insult, and it is followed by secondary processes including ischemia, anoxia, free radical formation and excitotoxicity that occur over hours and days after injury.[1] Furthermore, axonal regeneration in the CNS is hampered by myelin-associated inhibitors[1,2] and by the formation of a post-lesion scar barrier.[3] In most cases, chronicized SCI yields to extensive lost of spinal cord tissue that has to be replaced. Among others, in chronic and/or extensive SCI, various efforts have been focused on designing new biomaterials capable of stimulating axonal regeneration when delivered at the site of injury by providing permissive microenvironments mimicking the native extracellular matrix.[4]

In this regard, self-assembling peptide (SAP)[5–7] hydrogels are particularly appealing since they have various advantages: 1) their complex nanostructures can be assembled from peptidic building-blocks, that in turn are synthesized by aminoacid precursors; 2) self-assembly is usually triggered by pH and/or temperature shifts and no harmful chemical reaction is involved; 3) SAP biological activity can be modified by the inclusion of bioactive sequences, such as cell adhesion motifs; 4) SAPs may display multiple functionalizations enabling multi-faceted customized therapies targeting cells, drugs and tissues. Over the past two decades, various SAPs have been designed to spontaneously self-assemble into hierarchical structures ranging from β-sheets and nanotapes up to ribbons, fibrils and fibers.[8,9] A drawback of stimuli-triggered self-assembly peptides is that the required shift of pH, temperature or ionic strength, may not be compatible with physiological conditions suited for effective cell transplantation and/or drug delivery therapies, thus harming the biological drug/cell to be delivered with the self-assembling hydrogel. An alternative approach is to use a binary system in which two self-repulsive complementary charged peptides give

Dr. A. Raspa, Dr. G. A. A. Saracino, D. Silva, Dr. D. Cigognini, Dr. F. Gelain
Center for Nanomedicine and Tissue Engineering (CNTE)
A.O. Ospedale Niguarda Ca' Granda
Piazza dell'ospedale maggiore 3 20162, Milan, Italy
E-mail: gelain@mit.edu
Dr. G. A. A. Saracino, R. Pugliese, D. Silva
Biotechnology and Biosciences Department
University of Milan-Bicocca
Piazza della Scienza 2, Milan 20126, Italy
Dr. D. Cigognini
Network of Excellence for Functional Biomaterials (NFB)
Biosciences Building NUI
Galway, Ireland
Prof. A. Vescovi, F. Gelain
IRCCS Casa Sollievo della Sofferenza
Opera di San Pio da Pietrelcina
Viale Cappuccini 1, San Giovanni Rotondo (FG) 71013, Italy

DOI: 10.1002/adfm.201400956

rise to co-assembly upon mixing and to hydrogelation. This modular design strategy, based on mutual-attraction but self-repulsion of oligopeptides, has been documented by Yu and colleagues.[10] In their studies they showed that complementary co-assembling peptide (CAP) hydrogels exhibit a nanofibrillar network structure, high elasticity and shear-thinning nature. Most importantly, Yu's group demonstrated that mixing-induced material co-assembly is better at preserving the native conformation of biomolecules entrapped in the hydrogels, as the gelation process does not involve changes in pH, ionic strength, or temperature.[5,10] In more details, oppositely charged polyelectrolytes spontaneously aggregate because of non covalent interactions (electrostatic attractions, hydrophobic collapse, etc.).[11–13] Aggregation leads to large-scale superstructures yielding to hydrogels whose performance depends on the interplay of several factors: balance,[14] density and distribution[15] of positive/negative charges, length, and stiffness of the polyelectrolyte chains,[16,17] pH and ionic strength of the solution.[13] Because of their potential for regenerative medicine applications CAPs need in-depth studies: however aggregation dynamics of complex molecular structures are generally beyond the limits of a single technique. In particular, coarse-grained (CG) molecular dynamics (MD), representing a handful of atoms as a single grain and thus reducing the degrees of freedom of a molecular system, allow to investigate phenomena taking place on time and length scales beyond capacities of full-atom models: however their prediction is limited to small systems and time frames when compared to those of regenerative medicine.

In this study we combined coarse-grained molecular dynamics[18–21] with empirical experiments in vitro and in vivo to describe respectively the dynamics of aggregation of CAPs and their potential as scaffolds for stem cell culturing and spinal cord regeneration.

Here we showed that the co-assembly of complementary peptides is a promising method to build biomimetic nanoscaffolds for tissue regeneration. CG MD simulations together with characterization experiments (circular dichroism (CD), atomic force microscopy (AFM) and rheometry) evidenced the propensity of the chosen CAPs to co-assemble in bilayered aggregates and to form nanostructured shear-thinning hydrogels. In in vitro experiments CAPs supported neural stem cells (NSCs) viability and differentiation, while in an animal model of severe complete spinal cord transections they stimulated nervous regeneration. Our data suggest CAPs can be customized to achieve neural regeneration in complete SCI and, potentially, the regeneration of other tissues.

2. Results and Discussion

The different steps of the multidisciplinary "full" bottom-up approach we used are described and discussed following the strategy we previously proposed.[7] Firstly, the propensity of the chosen CAPs (Section 2.1) to form nanostructured aggregates was investigated in silico (Section 2.2), followed by characterization tests assessing secondary structure of molecular aggregates, morphology of the assembled nanostructures and biomechanical properties of the hydrogels (Section 2.3). Then the neuro-regenerative potential of CAP scaffolds has been verified by assessing their effect over human and murine NSC (hNSC and mNSC) cultures (Section 2.4) and, lastly, in completely severed spinal cords (Section 2.5).

2.1. CAP Design

In this study we opted for a modular design strategy based on mutual-attraction and self-repulsion of positive (LKLK12) and negative (LDLD12) modules. We tested self-repulsive complementary charged peptide pairs: LDLD12 + LKLK12 and KLP-LDLD12 + LKLK12 (see **Table 1**). The former pair can be viewed as derived by the partitioning of the charged residues found in LDLK12 peptide, a well-known SAP in material science and tissue engineering,[22–24] into two separate peptides (modules). The two modules are composed of neutral leucines (L) alternating with positively or negatively charged amino acids, respectively lysines (K) and aspartic acids (D). The latter pair has been chosen to assess the feasibility of CAP functionalization.

All sequences were acetylated and amidated at respectively the N-termini and C-termini. Self-repulsion of each module prevents uncontrolled spontaneous self-assembly, while electrostatic interactions between positively and negatively charged peptides drive their co-assembly and lead to hydrogelation. Therefore, positioning positive and negative charges into two separate modules causes a mutual attraction of opposite CAPs upon mixing, leading to the formation of a composite scaffold. Mixing-induced hydrogelation takes place in physiological conditions, thereby preserves the structural folding of proteins encapsulated within the hydrogels, as well as viability of seeded cells, both desired properties for biomaterials.[10] Lastly, we functionalized the negatively charged sequence with the KLPGWSG functional motif, involved in both stem cell maintenance and differentiation. As previously shown,[25] KLPGWSG binds to molecules expressed on the cell surface of murine adult neural stem cells and is likely to be involved in stem cell fate determination. To improve the exposure of the functional motifs, a spacer of three-glycines was interposed between the functional motifs and the LDLD12 core.[26] In order to partially compensate the unbalanced negatively charged LDLD12 with the positively charged KLPGWSG this last option was preferred to positive module functionalization. The rationale of the overall following sections underlies in testing the feasibility of both complementary CAPs and of their functionalization.

Table 1. Sequence abbreviation and color legend of complementary peptides. For sake of simplicity color legend of LDLD12 and KLP-LDLD12 are the same. The color legend for co-assembled peptides is reported.

Sequence	Abbreviation	Color legend
Ac-LKLKLKLKLKLK-CONH2	LKLK12	Red
Ac-LDLDLDLDLDLD-CONH2	LDLD12	Blue
Ac-KLPGWSG-LDLDLDLDLDLD-CONH2	KLP-LDLD12	
COMPOSITE HYDROGEL	LDLD12 + LKLK12	Red and Blue
	KLP-LDLD12 + LKLK12	

2.2. Modeling of the Mixing-Induced Assembly of CAPs

Coarse-grained molecular dynamics simulations[18–21] have been used to investigate the mechanism and the quality of mixing-induced assembly of self-repulsive complementary charged peptides pairs shown in Table 1. The simulated systems reproduce the concentration conditions used in the CD experiments (see Supporting Information) where equal volumes of complementary peptides solutions at 1% w/v were mixed in presence of a low concentration of neutralizing agents (NaOH or HCl 0.025 M), thus resulting in final halved concentration for peptides, ions Na+ and Cl–. Lysines and aspartic acid side chains at neutral pH can be respectively considered fully protonated and deprotonated, according with their weak basic and acidic nature. All simulations have been performed using the CG force field Martini[27–29] and the initial conformation of all complementary segments (LKLK and LDLD modules) was set to extended (see Section 4 for details and Supporting Information Figure S1). We chose this option because of 1) the presence of equally spaced identical charges along the same short peptide chain,[30] 2) the presence of the oppositely charged CAPs after mixing and 3) the typical β-sheet signature in circular dichroism spectra showed by mixed CAPs (see Section 2.3). Additionally, a coil conformation has been used for the functional motif of the KLP-LDLD12 peptide because of the absence of a regular and close distribution of charges and the presence of four consecutive glycines, both conferring a high degree of conformational mobility. Two types of system, hereafter referred as mixed and unmixed (see **Figure 1**A), have been prepared. In the mixed systems the two CAPs are randomly positioned in the whole box, in the unmixed systems each type of CAP is confined in half box together with opposite charge ions (see Section 4). All systems were simulated for 4500 ns at 300 K and 1 atm in order to investigate the spontaneous propensity of the CAPs to aggregate. In both systems CAPs spontaneously co-assembled in bilayered blocks characterized by extended complementary backbones aligned and alternated. Hydrophobic side chains of leucines constituted an hydrophobic inner layer while charged (lysine and aspartic acid) side chains were exposed to the surrounding solvent (see Figure 1B).

Simulation studies revealed the spontaneous propensity of rod-like polyelectrolytes to adopt ribbon-like spatial organization in the presence of anisotropic counterions.[31] Bilayer morphology appears as the natural consequence of such a propensity when the main source of the counterion anisotropy lays on the presence of intercalating hydrophobic units (leucine residues in our case) driving the hydrophobic collapse.

In two out of three simulations the LDLD12 + LKLK12 pair (both in mixed and unmixed systems) assembled into big clusters collecting all peptide chains. We noticed a progressive recruitment of differently oriented blocks, yielding to a final aggregate constituted by a "patchwork" of peptides, where each “patch” shows clear features of alignment and alternation among complementary peptides. Growing aggregates often exhibit non-specular faces because the mutual orientation of the patches is different between the two layers (see Figure 1C). In summary, the co-assembly process proceeds through three main phases characterizing the evolution of polyelectrolyte complexes: 1) instantaneous formation of irregular primary complexes due to electrostatic binding interactions, 2) intra-complex arrangements from primary complexes to secondary complexes, 3) inter-complexes aggregation yielding bigger aggregates.[12]

To assess the alignment of peptides inside the aggregates, the nematic order parameter (P2) has been monitored along the simulations. According to the definition of this parameter (see Section 4), the propensity of peptides to mutual alignment and ordered aggregation may be recognized when its value exceeds 0.5. In our simulations P2 is generally less than 0.5 and exhibits oscillating trends until eventually plateauing. This trend is due to the formation of locally ordered floating patches changing their mutual orientation until final clustering (see Supporting Information Figure S2). Then, when final clusters are formed by merged patches, P2 variability decreases and is mainly given by intra-aggregate chain arrangements.

Because of the polyelectrolytic nature of the tested CAPs, the propensity of the different peptide couples to form steady aggregates cannot be exhaustively described by assessing their orientational order. In this perspective the complementary charges interspersion has been taken into account as well. We analyzed the complementary segment recruitment during simulations by monitoring different states of aggregation along the aggregation process (see Figure 1D and Section 4 for details). In the initial configuration all peptides are isolated (state I in Figure 1D) and each of them remains in such state until one or more of its backbone grains falls within a 4.5–6 Å distance from a backbone grain belonging to another peptide, thus passing in a contact state. This contact may be a low-contact state (state L in Figure 1D) if contacts are between no more than six backbone grains of the peptide pair. In case of contacts involving more than six backbone grains the two peptides are considered as aligned. Then we indicate two different alignments corresponding to the pairing between peptides bearing the same (state S in Figure 1D) or opposite net-charges (state D in of Figure 1D). Consequently, when a peptide chain is aligned with two peptides, its state can be double D, double S or mixed D and S (states DD, SS and DS in Figure 1D). The distance criterion we used detects contacts within the same sheet of a bilayer patch only, therefore the sheet terminal segments could only display D or S states while DD, SS as well as DS stand for sheet segments inside the patch.

According to the introduced schematization we extrapolated interesting parameters describing the global aggregation phenomena of the tested CAPs (Figure 1D): 1) the alternation degree “A” given by the sum of D and DD; 2) the percentage of defects (faults) “F” in respect to a perfectly alternated aggregate given by the sum of L, S, SS and DS; 3) the number of patches “P” representing the halved sum of the terminal segments D and S. These parameters described CAP integration and the formation/digestion process of the faults along the simulations.

Mixed systems exhibited a suddenly increase of A in a few tens of nanoseconds (ns) followed by a gradual shift from peptides in D state to peptides in DD states during the first 1500 ns, in accordance with the gradual decrease of the initial numerous small aggregates (high D) towards larger clusters (high DD). A similar shift was observed in unmixed system as well, however with an A increase less rapid than in mixed systems. The main difference between mixed and unmixed systems, however, lay

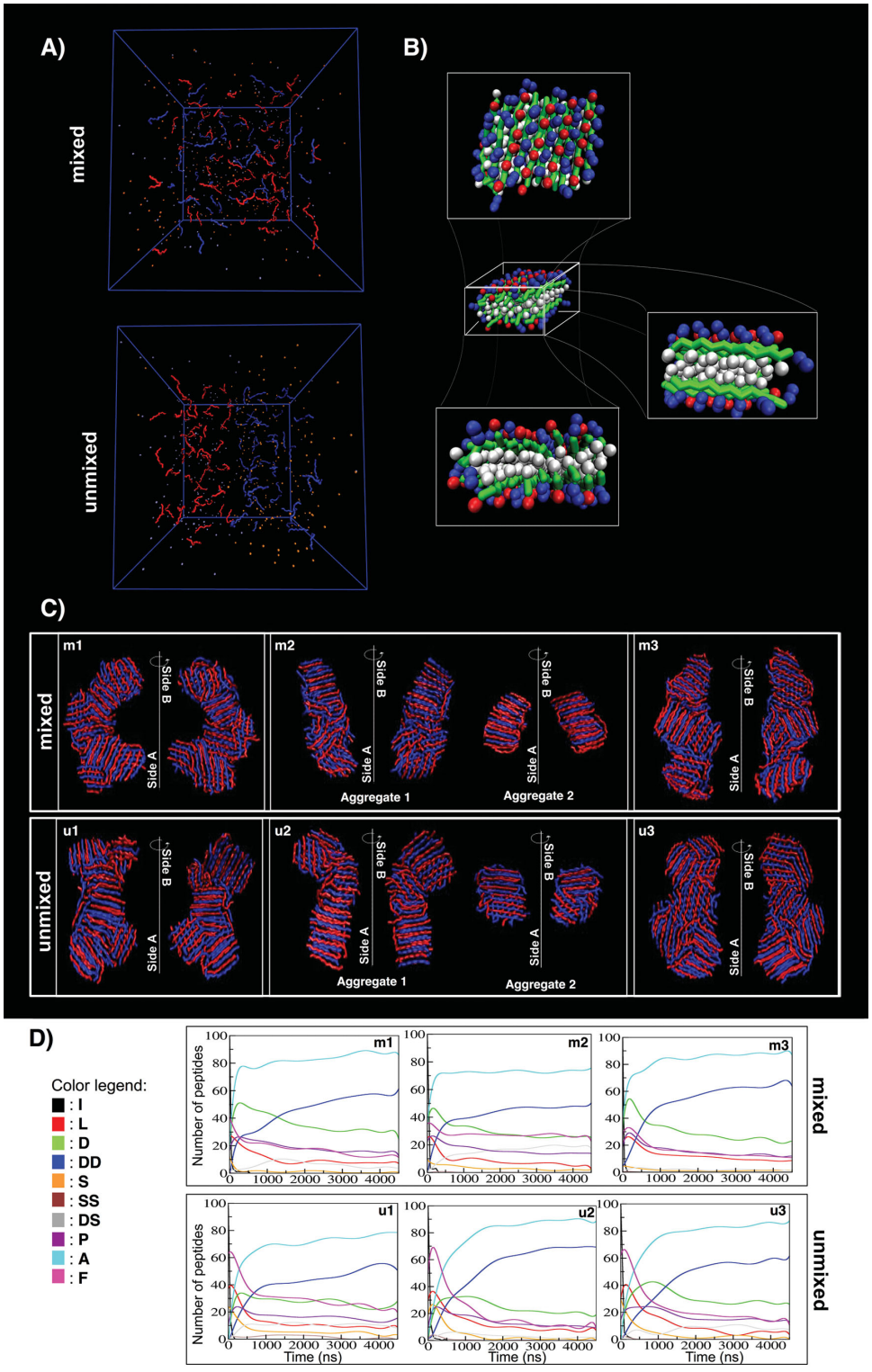

Figure 1. A) Initial configurations of the two simulated systems: mixed and unmixed. In the mixed system LKLK12 (blue) and LDLD12 (red) peptides, Na+ (iceblue) and Cl– (orange) ions are randomly positioned and oriented in the whole box. In the unmixed systems each type of peptide together with its complementary charged ion is randomly positioned in half box. B) Side-views and top-view of a portion of a double sheet co-assembled aggregate of LKLK12 + LDLD12 after simulation. Hydrophobic L (white) and both charged K (blue) and D (red) side chains are respectively positioned

in the formation/digestion process of defects. In unmixed systems, because of the initial confinement of each type of CAPs in its own half box, the overall aggregation phenomenon started with a spike of faults due to the formation of small aggregates made of identical peptides (self-aggregation) transiently stabilized by counter-ions. The 'digestion' of the defects arose from the aggregation of small clusters with complementary charged CAPs at the interface. On the other hand, in mixed systems, showing a more homogeneous distribution of the two types of CAPs, the initial spike of defects was less pronounced. The 'digestion' of defects steadily endured after the formation of the final aggregates both in mixed and unmixed systems because of the spontaneous arrangements of merged patch boundaries towards a better complementary charge alternation. The increase of the alternation degree, specular to the decrease of defects, then stabilized around 80%–90% but slowly decreased during the simulated timeframe.

Similar results were obtained for the pair LKLK12 + KLP-LDLD12 (see Supporting Information Figure S3A) with all simulations leading to final bilayered arrangements with alternated CAPs, further confirming the proper design of the chosen functionalization with KLP motif. The functional motifs are generally exposed to the solvent and rather uniformly distributed in the aggregates (regardless of the initial distribution of CAPs), *i.e.,* presumably available for cell membrane protein (and/or cytokine) interactions. Also in this case, the alternation degree (see Supporting Information Figure S3B) reached high values, confirming that the presence of the functional motif doesn't compromise the interspersion of the two types of peptides.

For all the above our modeling analysis show a spontaneous propensity of CAPs to aggregate in double layers formed by merging blocks of alternated positively and negatively charged peptides. The typical surface topography showed by final aggregates is given by the propensity of single clusters with different orientations to attach to each other and their subsequent tendency to improve the internal backbone chains alignment. This phenomenon is compatible with quick aggregation dynamics favorable to enlargements and ramifications, a crucial requirement to sustain three-dimensional scaffolding of hydrogels. In both LDLD12 + LKLK12 and KLP-LDLD12 + LKLK12 systems bilayers were generally 2 nm in thickness, in accordance with AFM data (see Section 2.3). Nonetheless final aggregate width (from 4–6 nm of aligned and stretched bilayers to 8 nm of branching points) may be in partial disagreement with measurements of nanofibers detected with AFM sample preparation and analysis. It is presumable to assume that CAP systems with higher complexity (i.e., with larger CAP population) and over longer periods of time (as in AFM characterization) may better organize into nanofibers made of side-by-side alignments of ordered aggregates (see section 2.3).

On the other hand the bilayered aggregates formed during the simulations are in agreement with the presence of beta structures observed in CD spectra (see the section below), therefore confirming the usefulness of in silico studies to predict and elucidate the co-assembly of CAPs.

2.3. Characterization of Assembled Nanostructures and Hydrogels

In the idea of analyzing the CAP properties at bigger and bigger scales first step is defining the secondary structures of the assembled aggregates, followed by morphological analysis of formed nano- and microstructures. Lastly, mechanical characterization of the assembled biomaterials has to be performed in order to elucidate visco-elastic parameters of the scaffolds at the meso-scale.[32]

Circular dichroism was used to study the secondary structure and folding of LKLK12 in pure water solution, of LDLD12 and KLP-LDLD12 in NaOH 25mM solutions (see the Experimental Section), and of co-assembled hydrogels. For sake of completeness, we must state that changes of ionic strength, as well as of pH, associated with the addition of NaOH might influence the physical properties of the individual peptides[33,34] and of their self- and co-assembling kinetics. The effect of different NaOH concentrations should be tested in future works. The CD spectra of each individual peptide solution showed a random coil minimum near 200 nm, thus suggesting unordered aggregations of same-type CAPs. A β-sheet signature appeared when the opposite charged peptides were mixed, showing a negative band near 215 nm and a positive band between 195 and 200 nm (**Figure 2**Ai). To confirm these data and analyze the effect of pH shift associated with mixing, a divided chamber cell was used (see Supporting Information). The obtained spectra showed that, also upon pH neutralization, β-sheet formation was detected only when opposite charged peptides were mixed and not when they were present individually (Figure 2Aii). In summary, in the timeframes chosen for these tests, the formation of a typical β-sheet structure required the co-assembly of opposite charged peptides and was not pH dependent.

Morphological analysis was carried out via AFM to detect the presence of nanofibers in CAP solutions.[35] Before the deposition on fresh mica each peptide solution was diluted to a final concentration of 0.1% w/v. Sparsed nano-rods and/or short nanofibers were observed in the samples containing a single type of peptide, as shown in Figure 2B. Mixed solutions, however, led to the formation of longer and much more numerous nanofibers if compared to individual CAP solutions. Morphometrical analysis showed that fibers of co-assembled peptides ranged from 10.2 ± 2.8 to 11.5 ± 2.5 nm and 2.4 ± 0.4 to 2.2 ± 0.2 nm respectively in width and height (Figure 2B). The dependency of self-assembling on pH shift was demonstrated by

inside and outside the double sheet composed by alternated LKLK12 and LDLD12 peptides. Backbones are green. C) Backbone framework of the aggregates formed after 4500 ns of simulation of both mixed (m1, m2, m3) and unmixed (u1, u2, u3) systems. The two faces of aggregates are non-specular and show a patchwork arrangement of their backbone framework. LKLK12 and LDLD12 backbones are marked in blue and red respectively. The formation of extended bilayer structures with multi-directional growing branches is in agreement with the presence of β-sheet signatures in CD spectra and with the formation of curly fibers seen in AFM images. D) Distribution of peptide aggregation states along the simulations (see code and color legend on the panel). The propensity of the systems towards higher ordered arrangements is shown by the increase of the alternation degree A (aligned and alternated peptides) as well by the decrease of the number of patches P and faults F (peptides either in low contact state or not aligned with complementary peptides).

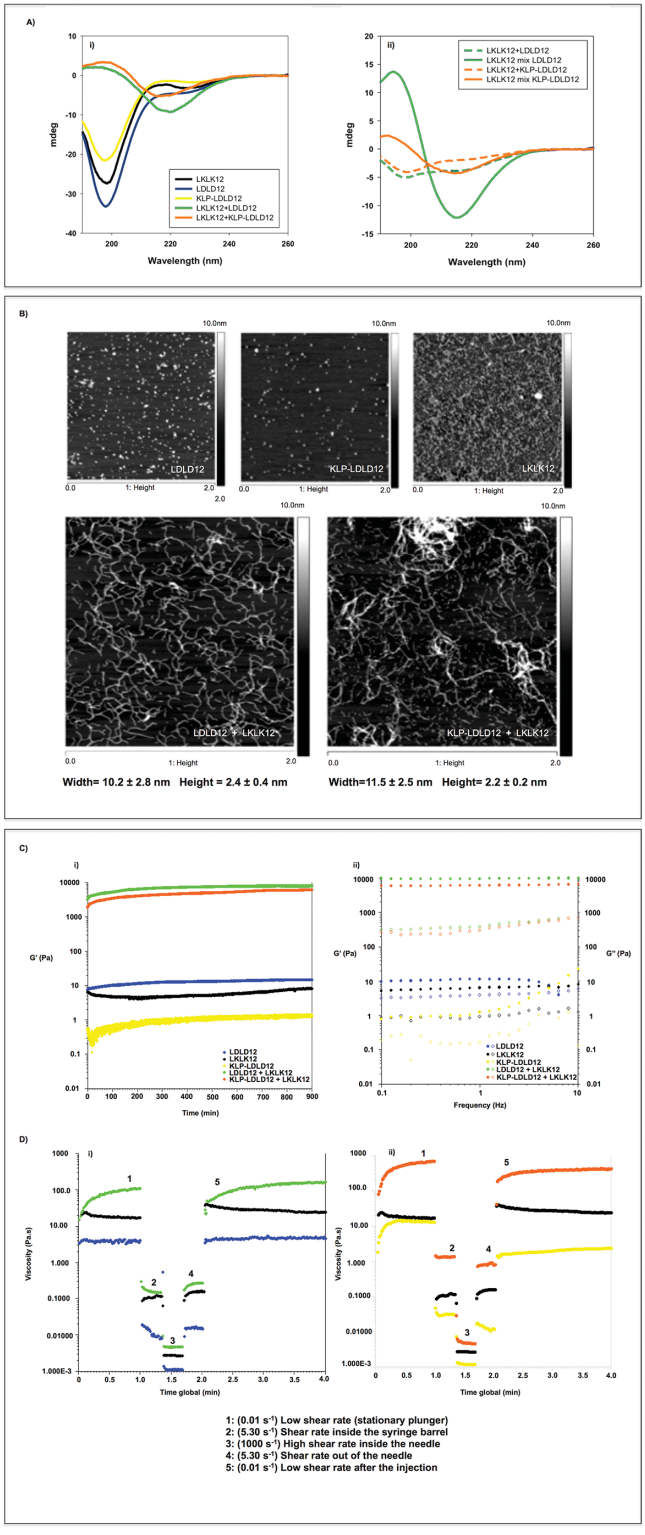

Figure 2. A) Far UV CD spectra of single CAPs and composite hydrogels formed by mixing the two CAP pairs: LDLD12 + LKLK12 and KLP-LDLD12 + LKLK12. CD analyses were carried out with a 1-mm quartz cuvette i) and a 1-cm divided chamber quartz cuvette ii). In i) same-type peptide solutions show an unordered structure profile (black, blue and yellow). A typical β-sheet signature appears when the opposite charged peptides are mixed (green and orange). Divided chamber cell was used to eliminate the effect of pH shift ii). Dashed lines represent the algebric sum of the spectra of separated CAPs; solid lines display the spectra of mixed and interacted CAPs. Green and orange solid lines indicated β-sheet presence in both composite hydrogels. B) Atomic force images of peptides LDLD12, KLP-LDLD12, LKLK12 and composite hydrogels. Average measures of assembled nanofibers are indicated. C) Rheological characterization of CAPs and composite hydrogels. Oscillation experiments consisted of an overnight time sweep test i) and a subsequent frequency sweep test ii). Composite hydrogels (green and orange) showed a significant increase of the storage modulus (G'). The typical hydrogel profile was confirmed in ii): solid-like component G' of co-assembled hydrogels (green and orange) resulted approximately one order of magnitude greater then the viscous component G''. D) Shear-thinning hydrogel assessment: injection simulation test. i) and ii) peak hold test performed with different constant shear rate values: 1 (0.01 s^{-1}) low shear rate (stationary plunger); 2 (5.30 s^{-1}) shear rate inside the syringe barrel; 3 (1000 s^{-1}) high shear rate inside the needle; 4 (5.30 s^{-1}) shear rate out of the needle; 5 (0.01 s^{-1}) low shear rate after the injection. Composite hydrogels exhibited higher viscosity values in respect to same-type CAP solutions.

mixing directly on the mica surface 1 µL of individual CAP solutions with 1 µL of 25 mM NaOH and of 25 mM HCl solutions, respectively for positively and negatively charged peptides (see Section 4). Intriguingly, results suggest that pH shift may trigger a weak self-assembly (see Supporting Information Figure S4), in accordance with a reduction of inter-chains repulsive effects given by ion screening, but is not sufficient to trigger the formation of stable structured scaffolds of same-type CAPs. However, in our opinion, these findings are not in contradiction of CD results. Indeed, CD analysis provides a cumulative analysis of the overall system (where a widely diffused random coil component may prevail over a small fraction of self-assembled peptides), while AFM imaging provides a detailed and focused view of samples that were subjected to washing steps, likely bringing away unaggregated peptides and/or random clusters (see Section 4 and Supporting Information Figure S4 for details).

After confirming the propensity of both composite hydrogels to form nanostructures, biomechanical properties of each peptide solutions were investigated via rheometry. Rheology is a branch of science that studies the mesoscopic properties of materials, evincing parameters helpful for the characterization of their viscoelasticity.[36] Important rheological parameters for the mechanical characterization of soft materials are the storage modulus (G') and loss modulus (G''). G' is correlated to the stiffness of the material and its increase as a function of time, frequency or strain can be indicative of structural and networking processes.[37,38] G'' corresponds to the energy dissipated during the characterization process and represents the liquid-like response of a sample. In the case of β-sheet rich peptide nanofibers, the growing presence of β-structures and the interactions among the fibers lead to formation of an entangled fibrous network, that provides increased values of G'.[36] Hence analyzing G' as a function of time gives information about overstructuring kinetics of peptides solutions. All pre-assembled solutions were monitored via time sweep test (see Section 4). Each peptide solution was monitored for 15 h and the G' measurements are shown in Figure 2Ci. As depicted, solutions of just positively or negatively charged peptides showed a low value of G' (G' ≅ 10 Pa), while composite hydrogels showed

high values of G', from 1000 to 10000 Pa, namely displaying hydrogel-like profiles with higher stiffness.

The progression of G' and its comparison with G'' was also monitored via frequency sweep test. The comparison between G' and G'' gives an indication of viscoelastic profile of the tested gel: a G'' greater than G' (tan $\delta > 1$) is typical of a viscous liquid, while a G'' smaller than G' (tan $\delta < 1$) represents an elastic solid like an assembled hydrogel.[39] The frequency sweep test performed on each sample of assembled scaffolds is represented in Figure 2Cii. The trend of G' and G'' for each peptide showed the typical profile of soft hydrogels, featuring a predominant solid-elastic behavior (G') as compared to the viscous component (G''): indeed G' values were generally one order of magnitude greater the G''. Though G' and G'' remained relatively constant along the frequency range (0.1–10 Hz) only co-assembled peptide hydrogels displayed significant increased values of the storage modulus (G'). Higher values of G' are probably due to higher organization of co-assembled hydrogels given by better packed molecular aggregations seen in CD experiments (beta-sheets), by nanofiber morphologies shown in AFM morpholgical tests. Notably, functionalization of CAPs with the KLPGWSG motif did not prevent high values of G', thus co-assembly (as expected from the results described in the previous section) and hydrogel formation.

To evaluate the propensity of materials to recover their initial viscosity after injection in vivo, the thixotropy of all solution was also investigated.[40] In these shear-thinning tests the injection conditions have been simulated through a series of constant shear rate tests (Figure 2D). All peptide solutions exhibited a fast recovery after injection simulation and evidenced the lower viscosity of single-type positively or negatively charged peptide solutions in comparison with composite hydrogels. The fast viscosity recovery after injection suggests a space-filling propensity of all CAPs, a desirable feature for tissue engineering applications.

2.4. CAPs as Cell Culture Substrates for Neural Stem Cells

The potential of CAPs as substrates for stem cell cultures has been tested in vitro. CAP hydrogels are transparent, and therefore appropriate for microscopic analyses. Direct observations of neural stem cells in hydrogel matrices were performed in 96 MW plates to facilitate high throughput analyses. We conducted in vitro tests to assess NSCs survival and differentiation over LDLD12 + LKLK12, KLP-LDLD12 + LKLK12 and Cultrex (positive control) substrates (see Section 4 for details). After 7 days in vivo (DIV) both human and murine cells cultured over assembled hydrogels showed spread, branched and fusiform shapes like maturing neural cells, as showed by bright-field microscopy images (data not shown). Cytotoxicity of CAPs was examined using the Live/Dead viability/ cytotoxicity assay (see Section 4 for details).

As shown in **Figure 3**A and Supporting Information Figure S5A, hNSC and mNSC live cells were stained in green while dead cells were marked in red. LDLD12 + LKLK12 exhibited 77.8 ± 5.0% of live hNSCs, while KLP-LDLD12 + LKLK12 and positive control Cultrex gave respectively 81.0 ± 2.4% and 90.5 ± 1.6% values. Statistical analysis showed a significant difference

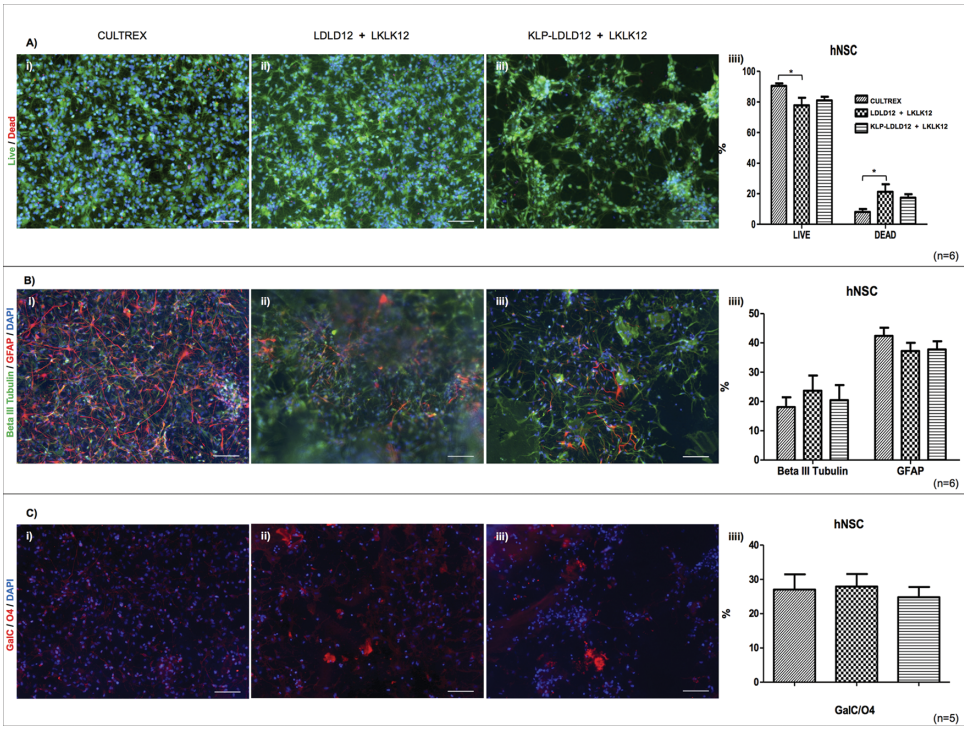

Figure 3. In vitro assays of hNSCs cultured on i) Cultrex, ii) LKLK12 + LDLD12 and iii) LKLK12 + KLP-LDLD12 at 7 DIV. Cell nuclei are visualized with DAPI (blue). A) Fluorescent viability/cytotoxicity assay: iiii) quantification of hNSC survival shows significant differences between LDLD12 + LKLK12 and Cultrex (* $p < 0.05$). B) Neural and astroglial differentiation assessment: iiii) quantification of hNSC differentiation shows no significant differences between CAP hydrogels and Cultrex for GFAP+ (red) and Beta III Tubulin+ (green) cells. C) Oligodendroglial differentiation assessment: quantification of GalC/O4+ cells (red) shows no significant difference between CAP hydrogels and Cultrex. Scale bars = 100 μm.

only between Cultrex and LDLD12 + LKLK12, however results are satisfactory for a fully synthetic and not functionalized substrate vs the animal-derived Cultrex. On the other hand, the percentage of live mNSC obtained on both composite hydrogels was comparable with results obtained on Cultrex (66.1 ± 1.3% for LDLD12 + LKLK12; 71.0 ± 1.9% for KLP-LDLD12 + LKLK12; 69.0 ± 6.7% for Cultrex), indicating that CAP hydrogels may be suited for stem cell cultures.

We then assessed the phenotype of differentiated hNSC and mNSC progenies (Figure 3 and Supporting Information Figure S5). hNSCs cultured on CAP hydrogels exhibited neural branching similar to that found on Cultrex. Cells were immunostained with markers for astrocytes (GFAP), post-mitotic neurons (Beta III Tubulin) and oligodendrocytes (GalC and O4). In case of hNSCs, LDLD12 + LKLK12 and KLP-LDLD12 + LKLK12 showed respectively 23.7 ± 5.2% and 20.4 ± 3.7% of cells positive to Beta III Tubulin (Figure 3Biiii); 37.2 ± 2.8% and 37.8 ± 2.8% positive to GFAP (Figure 3Biiii); 27.9 ± 3.7% and 24.8 ± 3.0% positive to GalC-O4 (Figure 3Ciiii). In case of Cultrex we detected 18.1 ± 3.3% of cells positive to Beta III Tubulin, 42.4 ± 2.8% to GFAP and 27.1 ± 4.4% to GalC-O4. Lacking any significant difference among the just mentioned results, LDLD12 + LKLK12 and KLP-LDLD12 + LKLK12 are comparable to positive control Cultrex in terms of differentiation potential of hNSCs. In case of mNSC differentiation no statistical difference among the tested substrates was detected for neuronal and oligodendrocyte stainings: LDLD12 + LKLK12, KLP-LDLD12 + LKLK12 and Cultrex gave respectively 13.2 ± 1.1%, 17.1 ± 3.6% and 18.4 ± 4.5% of cells positive to Beta III Tubulin+ (Supporting Information Figure S5Biiii) and 21.3 ± 3.5%, 22.7 ± 5.1% and 29.8 ± 7.9% of cells positive to GalC-O4 (Supporting Information Figure S5Ciiii). In case of astrocytes staining we detected 39.1 ± 1.1%, 48.5 ± 5.0% and 63.5 ± 5.3% of cells positive to GFAP for respectively LDLD12 + LKLK12, KLPLDLD12 + LKLK12 and Cultrex. Statistical analysis pointed out significant differences of GFAP+ murine cells cultured on Cultrex vs LDLD12 + LKLK12 (*significant different values $p < 0.05$) and Cultrex vs KLP-LDLD12 + LKLK12 (*** significant different values $p < 0.001$) (Supporting Information Figure S5Biiii). Immunofluorescence imaging of murine neurons, astrocytes and oligodendrocytes showed a highly organized network of neurons and astrocytes obtained on both Cultrex and CAP scaffolds. In the end, CAP hydrogels support NSC neural and oligodendroglial differentiation similarly to positive control Cultrex, a promising property for fully synthetic scaffolds enabling reproducible and well-defined cell culture conditions in vitro.

2.5. Neuroregenerative Potential of CAPs in Complete Spinal Cord Transections

Complete spinal cord transection was selected as a severe animal model for evaluating the neuroregenerative potential of CAP hydrogels in vivo.[41] Here, we attempted to reinstate an appropriate structural and regenerative milieu using CAP hydrogels together with electrospun guidance microchannels previously tested with SAPs (see Section 4 for details).[4]

Being the results of KLP-LDLD12 + LKLK12 in vitro not significantly different from LDLD12 + LKLK12 we preferred to focus all the experiments in vivo on the latter CAP with no functional motif. Animals received a dorsal laminectomy at T9-T10 level and the exposed spinal cord was transected leaving a 2 mm gap between the severed stumps. Then we sealed the lamina to the dura mater with fibrin glue to cover the gap (control group: $n = 7$) or we implanted the guidance channels filled with CAP hydrogel (experimental group: $n = 6$). Depending on the size of the lesion, 30–40 channels were implanted along the longitudinal spinal cord axis in order to fill the gap. Lastly an electrospun lamina (of identical chemical composition and similar fiber diameters to the guidance channel) was sutured to the dura mater and sealed with fibrin glue.

Three months after surgery the nature of the newly formed tissue was studied by immunohistochemical analysis. The whole cyst area was calculated by ImageJ software on Azan Thrichrome stained sections (see Section 4 for details).

The cyst area was 7.6 ± 2.8 mm^2 in control group and 6.2 ± 1.0 mm^2 in treated group (**Figure 4**A). Statistical analysis showed no significant differences between the two groups. The presence of glial cells, blood vessels and axons was quantified by ImageJ software on immunofluorescence stained sections. GFAP positive astrocytes formed an intense reactive glial border near the implant and were also found between the channels and inside their lumens. GFAP immunoreactivity in control group was 6.1 ± 1.1%, therefore comparable with 6.6 ± 0.7% reactivity detected in treated group (Figure 4Bi). Staining for Collagen IV, which is one of main components of basement membranes in nervous tissue, was conspicuous and widespread and was located within the tissue regenerated throughout the guidance microchannel inner lumens. Nonetheless, the reactivity for Collagen IV within the gap was similar between control (7.4 ± 0.9%) and treated (6.9 ± 0.5%) groups (Figure 4Bii). Scaffold implants became vascularized, as shown by the presence of many vWF positive blood vessels infiltrating the microchannels (see Figure S6, Supporting Information). Blood vessels were aligned along the longitudinal orientation of the channels while in control groups they were mainly absent, indicating that electrospun channels and CAP hydrogels favor the formation of a proper blood supply, desirable effect necessary to sustain healing and regenerative processes.

Analysis of GAP43 immunostaining revealed that the regenerating neuronal growth cones grew along the spinal cord axis (Figure 4Ci) as requested for the regeneration of the physiological cytoarchitecture. The immunoreactivity for GAP43 was 10.2 ± 0.9% in treated animals and 1.7 ± 0.4% in control group. Statistical analysis showed a significant difference for GAP43 in favor of animals receiving CAP hydrogels compared to control animals. Newly formed nervous fibers grew from both the proximal and distal ends of the lesion inward the implant. Nervous fibers were found at the tissue-implant borders and within of the implants, and in most cases they infiltrated large portions of the guidance microchannels. Within the guidance conduits, regenerating axons were positive for SMI31 immunostaining. SMI31 is a neuronal marker for phosphorylated neurofilament H of axons and a marker of axonal maturity.[42] Numerous SMI31 immunopositive axons grew in fascicles and aligned longitudinally along the axis of the guidance channels,

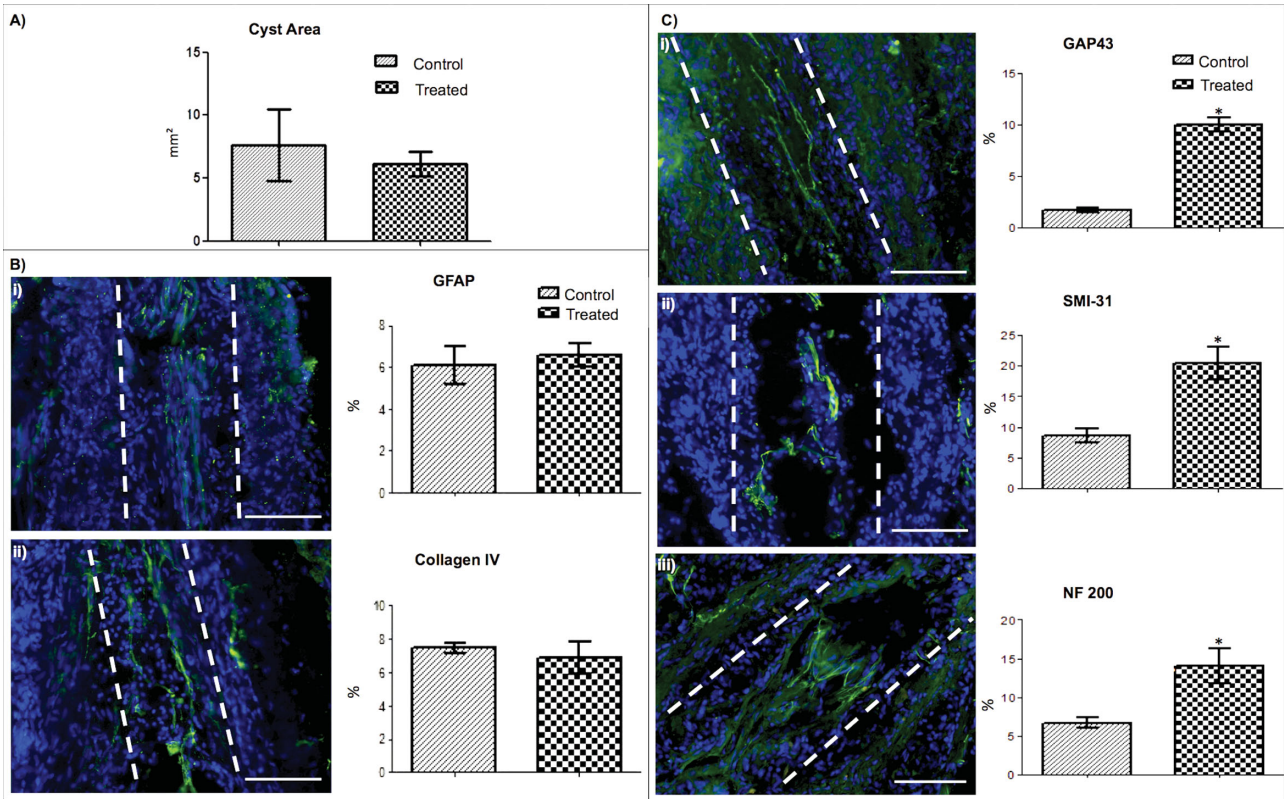

Figure 4. In vivo spinal cord injury regeneration assessment. A) Cyst areas were quantified on spinal cord longitudinal sections and no significant difference was found between control and treated groups. B) i) GFAP$^+$ glial cells surrounding and infiltrating the electrospun microchannels. ii) Collagen IV deposition within the guidance channels. No significant difference between the groups was found. C) Pixel area positive to neuronal markers. Higher values of i) GAP-43, ii) SMI-31, iii) NF-200 positive fibers were detected in treated group than in control group. Values = mean ± SEM. Scale bars = 100 μm. (* $p < 0.05$). Dashed lines outline channel walls in the reported longitudinal sections of the implanted scaffold.

covering the entire length of the implants. Axonal regeneration into the injury site highly correlated with the presence of CAP hydrogel and microchannels: we found a significantly greater synthesis of SMI31 in animals with implants (19.6 ± 0.3%) in comparison with control group (8.6 ± 0.2%) (Figure 4Cii). NF200 immunolabeling revealed that neurofilaments grew into the guidance channels in an interestingly linear manner (Figure 4Ciii). Very few NF axons were observed in the control group. We measured the percentage of NF200 positive fibers in treated animals (14.1 ± 3.3%) and in control group (6.7 ± 1.0%): statistical analysis showed a significant difference for NF200 in favor of treated animals. We assume that these neurofilaments may arise from regenerating long axonal tracts and local neuronal sprouting. Overall, the significant increase of infiltrating nervous fibers, blood vessels, GFAP positive cells and Collagen IV deposition within the implants suggests that LDLD12 + LKLK12 constituted a permissive microenvironment for the regeneration of tissue of the Central Nervous System. Additionally, we reiterated the fruitful usage of electrospun microchannels to spatially guide regenerating nervous fibers from side to side of the lesion.[4] In our previous studies we also reported that in spinal cord injures axonal regeneration was still active six months after grafting nanostructured composite scaffolds,[4] and that SAP scaffolds further improve their regenerative performance if loaded with drugs: therefore the next step will be to ameliorate the obtained in vivo data by choosing longer experimental timeframes and implanting CAP hydrogels seeded with NSCs loaded with neurotrophic factors.

3. Conclusions

In this work we faced the molecular design and assessed the molecular aggregation dynamics in silico of novel co-assembling peptides. The performed coarse-grained molecular dynamics showed the propensity of CAPs to co-assemble and co-integrate in double layers. The theoretical results were consistent with empirical data (AFM and CD) and suggested us to introduce biofunctionalization to one co-assembling sequence. By characterization analyses we confirmed CAP co-assembling propensity and by thixotropy tests we evidenced their fast recovery of viscosity, suggesting a space-filling propensity after injection useful for tissue engineering applications like brain ischemic injury, spinal cord injury and bone fillers. CAPs were tested in vitro and we demonstrated their encouraging interaction (comparable to positive control) with differentiating human and murine NSCs. Lastly we demonstrated CAP regenerative potential in stimulating nervous regeneration in complete spinal cord transections in vivo.

Aware that further in vivo tests with functionalized peptides are essential to assess the effectiveness of functional motifs to

increase the axonal regenerative ability, the obtained results are encouraging enough to push forward the research on CAPs for nervous regeneration treatments. Indeed it would be interesting to test the stability of the obtained CG aggregates in all-atom systems or to enhance the sampling space by using appropriate techniques like parallel tempering.[43,44] The "full" bottom-up approach here presented gives a first wide glimpse of the LDLD12 and LKLK12 systems but other issues have still to be answered (e.g., ion interference over co-assembled structure formation, feasibility to multiple functionalization, CAPs interactions with SAPs in case of assembling of complex systems, etc.). Nonetheless the insights we gained about the co-assembly mechanism, structural arrangements and mechanical properties of the scaffolds could be useful to design and develop new promising hydrogels for the treatment of SCI and novel co-assembling peptides (available for functionalization) for other tissue engineering applications.

4. Experimental Section

Molecular Aggregation Assessment: All-trans configuration of the peptides LDLD12, LKLK12 and KLP-LDLD12 (see Table 1) has been generated by PyMol (http://www.pymol.org) and minimized by the all-atom force field Amber99SB.[45] Subsequently, for each couple of CAPs, LDLD12 + LKLK12 and KLP-LDLD12 + LKLK12, peptides and ions (Na+ and Cl–) are introduced in an explicit water cubic box with 29-nm edge in such a number to simulate CD used concentrations (1% w/v and 0.025 M ion concentration respectively) to build two types of systems: 1) mixed, both complementary peptides and the ions were randomly distributed in the whole box; 2) unmixed, the random distribution of each complementary peptides together with the opposite chargeds ion were confined to half-box. Peptides were located so that atoms belonging to different peptides were at least at 6 Å far from each other. Systems were then translated into the coarse-grained model according with the version 2.2 of the MARTINI force field)[27,28] optimized to reproduce the behavior of multi-peptide systems.[29] The coarse-grained mapping[28,29] of each peptide is showed in Figure S1 of Supporting Information. All simulations were performed using the version 4.5.5 of the GROMACS package.[46] In case of the complementary couple LDLD12 + LKLK12 three simulations were performed for each systems, while for KLP-LDLD12 + LKLK12 the simulations were one for each. Extended secondary structures were imposed to all residues apart from the functional motif of the KLP-LDLD12, for which coil parameters were adopted. Unconstrained production simulations of the equilibrated systems (the equilibration procedure is reported in Supporting Informations) were carried out in isothermal-isobaric ensemble at 300 K and 1 atm by means of v-rescale method[47] (coupling constant of 1 ps) and Berendsen algorithm[48] (coupling constant of 2 ps) respectively. The total length of each production simulation is 4.5 μs that can be roughly compared with 18 μs atomistic simulation time.[27] An integration time of 20 fs is used and snapshots were saved at each 100 ps. Electrostatic interactions and Lennard-Jones potentials are modeled with shifted functions at 0.0–1.2 nm and 0.9–1.2 nm respectively. The alignment of the peptides during the simulations was monitored via the nematic order parameter calculated by the Wordom package.[49] The CAP alternation along the aggregation process was described by monitoring the aggregation state of each peptide as discussed in the Section 2.2 (see also Figure 1D and Supporting Information).

CAP Synthesis and Purification: Co-assembling peptides (LKLK12, LDLD12 and KLP-LDLD12) were synthesized via solid phase synthesis (Fmoc-chemistry) using the Liberty-Discover (CEM) microwave automated synthesizer. The solid substrate was the Rink amide resin (Fluka, 0.6 mmol g^{-1} substitution) and, accordingly, the C-terminal of each peptides was amidated after the cleavage of the peptide sequence. N-terminal was acetylated using a 20% solution of acetic anhydride in DMF. Activator and activator base solutions were respectively 0.5 M HBTU in DMF and 2 M DIEA in NMP while Fmoc-protected aminoacid solutions were solved at 0.2 M in DMF. Fmoc groups were removed by using a deprotection mix (20% v/v solution of 4-metylpiperidin in DMF). Peptide side chains removal and cleavage was performed with a solution of 95% TFA, 2.5% water and 2.5% triisopropylsilane. Raw peptides were purified with a Waters binary HPLC (>95%) and molecular weights were confirmed via single quadrupole mass detection (Waters LC-MS Alliance-3100). Positively charged peptide (LKLK12) was subsequently dissolved in 0.1 M HCl solution in order to remove TFA salt.

Rheological Test: Rheological properties of CAP solutions and hydrogels were investigated with an AR-2000ex (TA instruments) equipped with a truncated cone-plate geometry. The technical specifications for the acrylic truncated cone were: diameter, 20 mm; truncation, 34 μm; angle, 1%. The lower plate of the instrument was a Peltier cell used to keep controlled the temperature (25 °C) during each tests. Positively (LKLK12) and negatively (LDLD12 and KLP-LDLD12) charged peptides were dissolved at 1% w/v concentration the day prior the analysis. LKLK12 was solved in distilled water (GIBCO) whereas LDLD12 and KLP-LDLD12, due to their poor solubility in pure water, were solved in 25 mM solution of NaOH in distilled water (GIBCO). The final pH of positively (LKLK12) and negatively (LDLD12 and KLP-LDLD12) charged peptides, prior to the measurement, is respectively 6 and 7. Single charged peptides and composite hydrogel were analyzed. Composite hydrogels were obtained by mixing 1/1 the two opposite charged peptides directly on rheometer plate (24 μL + 24 μL, pH 7). These preparations of individual peptides and composite hydrogel are used also in CD and AFM measurements. A strain sweep test (0.1 to 1000% strain range) was first performed to identify the linear viscoelastic region (1% strain). After that a 15 h time sweep test was carried out in order to evaluate the storage modulus (G') increase as a function of time. Afterwards, a frequency sweep test (0,1 to 10 Hz, 1% strain) was run for the identification of both G' (storage modulus) and G'' (loss modulus). To confirm the formation of shear-thinning hydrogels we performed a flow test. Flow test consisted in a injection procedure simulation[40] aimed to assess the viscosity of single peptide and composite solutions. In all rheological tests, a mineral oil was placed laterally around peptide solutions in order to eliminate water evaporation.

Atomic Force Microscope Analysis: The microscope used for the analysis was a Multimode Nanoscope V (Digital Instruments, Veeco); images were captured in tapping mode and the probes were Veeco RFESP MPP-21100–10 (cantilever f0, 59–69 KHz; constant force: 3 N m^{-1}). CAP solutions were dissolved as previously described in Rheological test. Before the deposition of samples on a freshly cleaved mica surface, peptides solutions were diluted to final the concentration of 0.1 w/v. For each peptide 2 μL of solution were kept on mica for 2 min at RT and subsequently the surface was washed with distilled water. To trigger the formation of the composite hydrogel, 1 μL of both CAP solutions was placed and mixed on the mica surface. Also in this case solutions were let on the mica for 2 min and subsequently washed. Self-assembling propensity triggered by pH shifts was assessed by mixing directly on the mica surface 1 μL of peptide solution and 1 μL of 25 mM of NaOH and HCl solutions, respectively for positively and negatively charged peptides. As previously described 100 different nanostructures were measured on approximately 10 independent images and subsequently deconvolved.[50]

Circular Dichroism Analysis: Far UV CD spectra were collected in continuous scanning mode (190 and 260 nm) on Aviv 62DS spectrometer. All CD spectra were averaged over three accumulations (speed: 10 nm/min). Cells used for the analysis were a 1-mm quartz cuvette and 1-cm quartz cuvette with two divided chambers. Further details are reported in the Supporting Information.

Production of PCL/PLGA Microtubes for Neural Tissue Engineering: As previously described[4] a solution of 5.5% poly (ε-caprolactone) (PCL MW 80 000, Sigma-Aldrich) and 4% (w/w) poly (DL-lactide-co-glycolide) (PLGA, 75:25 MW 66 000–107 000, Sigma-Aldrich) in chloroform:

methanol (3:1) was used to create electrospun guidance microchannels and laminae. Spinal cord guidance microtubes were synthesized by depositing electrospun fibers on grounded 4 cm 33G microneedles with an outer diameter of 210 μm (Hamilton) for 15 s. Fibers were deposited but actually did not adhere to the microneedles. Needles were rotated at a speed of 36 rpm during fiber deposition in order to ensure uniform coating. The PLGA provides short-term strength, and the PCL provides long term stability.[51] Further details are reported in the Supporting Information.

NSC Cultures: Neural stem Cell cultures were established and expanded as previously described.[52] Briefly, murine NSC were isolated from the subventricular zone (SVZ) of 8-week-old CD-1 albino mice striata and cultured till passage 10. Human NSCs were isolated from the CNS, in particular the diencephalon and the cerebral cortex of human brain at 10.5 weeks from conception as previously described.[53] The modalities for obtaining the primary tissue are in agreement with the guidelines of the European Network for Transplantation (NECTAR). Further details are reported Supporting Information.

NSC Proliferation and Differentiation Assays: In vitro tests were performed adapting the procedure previously described for self-assembling peptides.[54] LKLK12 and LDLD12, KLP-LDLD12 CAPs were dissolved respectively in distilled water and 25 mM NaOH solutions at 1% w/v. CAPs (total volume of 30 μL/well at a total concentration of 10 mg mL^{-1}) were co-assembled in each well of 96 MW one hour before seeding cells by adding an initial layer of LKLK12 and subsequently the complementary CAP. Cells (at a concentration of 1 × 104 cells per cm^2) were seeded on the top-surface of each composite hydrogel after medium addition. For both survival and differentiation tests, basal medium supplemented with βFGF (10 ng mL^{-1}) has been used. After 7 DIV, the medium was changed with a medium containing Leukemia Inhibitory Factor (LIF, Chemicon) (20 ng mL^{-1}) and Brain Derived Neurotrophic Factor (BDNF, Peprotech) (20 ng mL^{-1}) to pursue the neuronal and glial population maturation in NSC progeny. For both viability and differentiation assays positive controls consisted of Cultrex-BME substrate (R&D systems) (1:100 dilution in basal medium). Cell viability was quantified via LIVE/DEAD kit (Molecular Probes) at 7 DIV as recommended in the manual instruction. Live cells were stained with green Calcein-AM, dead cells were identified by nucleic acid red dye Propidium Iodide. Cell Nuclei were stained with Hoechst 33342 (1:10 000, Molecular Probes). For immunofluorescence tests the following primary antibodies were used: rabbit anti-GFAP (1:500, DakoCytomation), mouse anti-Beta III Tubulin (1:500, Covance), mouse anti-GalC (1:200, Chemicon) and anti-O4 (1:200, Chemicon). Secondary antibodies were goat anti-Mouse Alexa 488 (1:1000, Molecular Probes), goat anti-Mouse Cy3 (1:1000, Jackson Immunoresearch), goat anti-Rabbit Cy3 (1:1000, Jackson Immunoresearch). Cell nuclei were counterstained with DAPI (Molecular Probes). Quantitative analyses were performed by counting 100–300 cells for each of 9 randomly chosen for each independent experiment. Fluorescence images of the adhering cells were acquired via Zeiss microscopes Axioplan 2 and ApoTome System.

In Vivo Animal Model: In spinal cord repair it is important to differentiate between axonal collateralization and true axonal regeneration. Hence, in order to focus our attention on the latter, a complete spinal cord transection was selected as a model for the evaluation of the neuroregenerative potential of CAP scaffolds on acute spinal cord injuries. 13 Female Sprague-Dawley rats (220–250 g body weight) from Charles River Laboratories were divided into two experimental groups. Immediately after spinal cord transection and removal of a 1 mm portion, 6 animals were implanted with CAP hydrogel injected into electrospun guidance microchannels (treated group), while 7 animals received only the electrospun lamina to cover the gap (control group). All procedures involving animals were performed according to EC guidelines (86/609/EEC), to the Italian legislation on animal experimentation (Decreto L.vo 116/92) and via protocols approved by the Animal Care and Use Committee of the University of Milano-Bicocca. Surgeries were performed via an OPMI-pico surgical microscope (Zeiss). Adult female Sprague-Dawley rats were anesthetized with an intraperitoneal injection of ketamine (80 mg kg^{-1}) and xylazine (10 mg kg^{-1}), then a 2 cm longitudinal skin incision was centered over the T9-T10 spinous process along the midline. Without disrupting the dura mater, T10 spinal segment was exposed by removing the dorsal part of the vertebra and the dura was incised longitudinally. The spinal cord was completely transected and a 1-mm segment of spinal cord was removed. The rostral and caudal stumps were lifted to ensure complete transection. The stumps then spontaneously retracted making a 2.0-mm gap in the spinal cord. When bleeding has stopped, we simultaneously injected onto the ventral dura drops of LDLD12 and of LKLK12 CAP solutions so as to initiate in situ hydrogel formation, then we inserted the electrospun tubes. Microchannels have been previously soaked with LKLK12 (1% w/v solution in distilled water) and then filled with LDLD12 (1% w/v solution in 25 mM NaOH) so as to allow the immediate in situ formation of the composite hydrogel. After a few minutes the guidance channels were inserted one by one into the gap forming 3–4 layers, aligned along the longitudinal spinal cord axis. Between each layer of tubes we co-injected drops of LDLD12 and LKLK12 solutions to trigger hydrogel formation. Upon filling of the gap we covered the microchannels and lesion margins with an electrospun lamina (of identical composition and similar fiber diameters to the guidance conduits) and sealed the lamina to the dura with fibrin glue. Subsequently muscles and skin were sutured. All rats were kept in low-sided cages to enable them easy access to food and water. Bladder expression was performed until the recovery of sphincter control. Animals were sacrificed after 3 months: at this time microchannels are still present and visible in bright field, while CAP hydrogels could be spotted in the blue field because of their auto-fluorescence.

Immunohistochemistry: See Supporting Information.

Overall Statistical Analysis: Data were processed using GraphPad Prism 5 software. Values are reported as means ± standard error of the mean (SEM). All in vitro results were analyzed via one-way ANOVA followed by the Tukey multiple comparisons test, with statistical significance set at $P < 0.05$. In the in vivo study, significance between treated and control groups was assessed via Student's *t*-test.

Supporting Information

Supporting Information is available from the Wiley Online Library or from the author.

Acknowledgements

A.R. and G.A.A.S. contributed equally to this work. This work was supported by Fondazione Cariplo, grant no. 2011–0352, by the "Ricerca Corrente 2011" funding granted by the Italian Ministry of Health and by the "5 × 1000" voluntary contributions. The authors thank Marchini A. for technical support.

Received: March 25, 2014
Revised: June 27, 2014
Published online: August 19, 2014

[1] M. S. Beattie, A. A. Farooqui, J. C. Bresnahan, *J. Neurotrauma* **2000**, *17*, 915.
[2] M. S. Chen, A. B. Huber, M. E. van der Haar, M. Frank, L. Schnell, A. A. Spillmann, F. Christ, M. E. Schwab, *Nature* **2000**, *403*, 434.
[3] D. Cai, J. Qiu, Z. Cao, M. McAtee, B. S. Bregman, M. T. Filbin, *J. Neurosci.* **2001**, *21*, 4731.
[4] F. Gelain, S. Panseri, S. Antonini, C. Cunha, M. Donega, J. Lowery, F. Taraballi, G. Cerri, M. Montagna, F. Baldissera, A. Vescovi, *ACS Nano* **2011**, *5*, 227.
[5] S. Maude, E. Ingham, A. Aggeli, *Nanomedicine* **2013**, *8*, 823.

[6] M. Nune, P. Kumaraswamy, U. M. Krishnan, S. Sethuraman, *Curr. Protein. Pept. Sci.* **2013**, *14*, 70.
[7] G. A. A. Saracino, D. Cigognini, D. Silva, A. Caprini, F. Gelain, *Chem. Soc. Rev.* **2013**, *42*, 38.
[8] S. Zhang, *Nat. Biotechnol.* **2003**, *21*, 1171.
[9] M. Sunde, L. C. Serpell, M. Bartlam, P. E. Fraser, M. B. Pepys, C. C. Blake, *J. Mol. Biol.* **1997**, *273*, 729.
[10] S. Ramachandran, Y. Tseng, Y. B. Yu, *Biomacromolecules* **2005**, *6*, 1316.
[11] J. van der Gucht, E. Spruijt, M. Lemmers, M. A. Cohen Stuart, *J. Colloid. Interface Sci.* **2011**, *361*, 407.
[12] E. Tsuchida, *J. Macromol. Sci. A* **1994**, *31*, 15.
[13] D. Priftis, M. Tirrel, *Soft Matter* **2012**, *8*, 9396.
[14] Y. Hayashi, M. Ullner, P. Linse, *J. Chem. Phys.* **2002**, *116*, 11.
[15] H. K. Murnen, A. M. Rosales, A. V. Dobrynin, R. N. Zuckermann, R. A. Segalman, *Soft Matter* **2013**, *9*, 9.
[16] A. A. Lazutin, A. N. Semenov, V. V. Vasilevskaya, *Macromol. Theory Simul.* **2012**, *21*, 12.
[17] C. F. Narambuena, E. P. M. Leiva, M. Chávez-Páez, E. Pérez, *Polymer* **2010**, *51*, 10.
[18] M. G. Saunders, G. A. Voth, *Annu. Rev. Biophys.* **2013**, *42*, 73.
[19] M. Baaden, S. J. Marrink, *Curr. Opin. Struct. Biol.* **2013**, *23*, 878.
[20] C. Wu, J. E. Shea, *Curr. Opin. Struct. Biol.* **2011**, *21*, 209.
[21] H. I. Ingólfsson, C. A. Lopez, J. J. Uusitalo, D. H. de Jong, S. M. Gopal, X. Periole, S. J. Marrink, *WIREs Comput. Mol. Sci.* **2013**, *24*.
[22] A. L. Sieminski, C. E. Semino, H. Gong, R. D. Kamm, *J. Biomed. Mater. Res. A* **2008**, *87*, 494.
[23] J. Sun, Q. Zheng, *J. Huazhong Univ. Sci. Technol. Med. Sci.* **2009**, *29*, 512.
[24] J. Sun, Q. Zheng, Y. Wu, Y. Liu, X. Guo, W. Wu, *J. Huazhong Univ. Sci. Technol. Med. Sci.* **2010**, *30*, 173.
[25] A. Caprini, D. Silva, I. Zanoni, C. Cunha, C. Volonte, A. Vescovi, F. Gelain, *N. Biotechnol.* **2013**, *30*, 552.
[26] F. Taraballi, A. Natalello, M. Campione, O. Villa, S. M. Doglia, A. Paleari, F. Gelain, *Front. Neuroeng.* **2010**, *3*, 1.
[27] S. J. Marrink, H. J. Risselada, S. Yefimov, D. P. Tieleman, A. H. de Vries, *J. Phys. Chem. B* **2007**, *111*, 7812.
[28] L. Monticelli, S. K. Kandasamy, X. Periole, R. G. Larson, D. P. Tieleman, S. J. Marrink, *J. Chem. Theory Comput.* **2008**, *4*, 819.
[29] D. H. de Jong, G. Singh, W. F. D. Bennett, C. Arnarez, T. A. Wassenaar, L. V. Schafer, X. Periole, D. P. Tieleman, S. J. Marrink, *J. Chem. Theory Comput.* **2013**, *9*, 687.
[30] J. L. Barrat, J. F. Joanny, *Europhys. Lett.* **1993**, *24*, 6.
[31] P. V. Komarov, L. V. Zherenkova, P. G. Khalatur, P. Reineker, *J. Chem. Phys.* **2006**, *125*, 154906.
[32] G. A. A. Saracino, D. Cigognini, D. Silva, A. Caprini, F. Gelain, *Chem. Soc. Rev.* **2013**, *42*, 225.
[33] M. R. Caplan, P. N. Moore, S. Zhang, R. D. Kamm, D. A. Lauffenburger, *Biomacromolecules* **2000**, *1*, 627.
[34] S. Förster, M. Schmidt, *Adv. Polym. Sci.* **1995**, *120*, 51.
[35] D. P. Allison, N. P. Mortensen, C. J. Sullivan, M. J. Doktycz, *Wiley Interdiscip. Rev. Nanomed. Nanobiotechnol.* **2010**, *2*, 618.
[36] C. Yan, D. J. Pochan, *Chem. Soc. Rev.* **2010**, *39*, 3528.
[37] H. D. Lu, M. B. Charati, I. L. Kim, J. A. Burdick, *Biomaterials* **2012**, *33*, 2145.
[38] A. Sein, J. A. Verheij, W. G. Agterof, *J. Colloid Interface Sci.* **2002**, *249*, 412.
[39] E. Genove, C. Shen, S. Zhang, C. E. Semino, *Biomaterials* **2005**, *26*, 3341.
[40] D. Cigognini, in *J. Biomed. Nanotechnol.* **2013**, Vol. *9*, 1.
[41] A. Hejcl, L. Urdzikova, J. Sedy, P. Lesny, M. Pradny, J. Michalek, M. Burian, M. Hajek, J. Zamecnik, P. Jendelova, E. Sykova, *J. Neurosurg. Spine.* **2008**, *8*, 67.
[42] R. L. Haynes, N. S. Borenstein, T. M. Desilva, R. D. Folkerth, L. G. Liu, J. J. Volpe, H. C. Kinney, *J. Comp. Neurol.* **2005**, *484*, 156.
[43] H. H. Tsai, M. Reches, C. J. Tsai, K. Gunasekaran, E. Gazit, R. Nussinov, *Proc. Natl. Acad. Sci. U.S.A.* **2005**, *102*, 8174.
[44] M. Cecchini, F. Rao, M. Seeber, A. Caflisch, *J. Chem. Phys.* **2004**, *121*, 10748.
[45] V. Hornak, R. Abel, A. Okur, B. Strockbine, A. Roitberg, C. Simmerling, *Proteins* **2006**, *65*, 712.
[46] D. Van Der Spoel, E. Lindahl, B. Hess, G. Groenhof, A. E. Mark, H. J. Berendsen, *J. Comput. Chem.* **2005**, *26*, 1701.
[47] G. Bussi, D. Donadio, M. Parrinello, *J. Chem. Phys.* **2007**, *126*, 014101.
[48] H. J. C. Berendsen, J. P. M. Postma, W. F. Vangunsteren, A. Dinola, J. R. Haak, *J. Chem. Phys.* **1984**, *81*, 3684.
[49] M. Seeber, M. Cecchini, F. Rao, G. Settanni, A. Caflisch, *Bioinformatics* **2007**, *23*, 2625.
[50] D. Silva, A. Natalello, B. Sanii, R. Vasita, G. Saracino, R. N. Zuckermann, S. M. Doglia, F. Gelain, *Nanoscale* **2013**, *5*, 704.
[51] H. Sun, L. Mei, C. Song, X. Cui, P. Wang, *Biomaterials* **2006**, *27*, 1735.
[52] A. L. Vescovi, B. A. Reynolds, D. D. Fraser, S. Weiss, *Neuron* **1993**, *11*, 951.
[53] A. L. Vescovi, E. A. Parati, A. Gritti, P. Poulin, M. Ferrario, E. Wanke, P. Frolichsthal-Schoeller, L. Cova, M. Arcellana-Panlilio, A. Colombo, R. Galli, *Exp. Neurol.* **1999**, *156*, 71.
[54] F. Gelain, D. Bottai, A. Vescovi, S. Zhang, *PLoS One* **2006**, *1*, e119.